Characterisation of the Ferrocene/Ferrocenium Ion Redox Couple as a Model Chemistry for Non-Aqueous Redox Flow Battery Research

Craig G. Armstrong, Ross W. Hogue, Kathryn E. Toghill*

Department of Chemistry, Lancaster University, Lancaster LA1 4YB, UK

*Corresponding Author: k.toghill@lancaster.ac.uk

Keywords

- Redox Flow Battery
- Non-aqueous
- Ferrocene model chemistry
- Capacity loss diagnosis
- Flow-cell diagnostics

Abstract

The simple ferrocene/ferrocenium ion ($Fc/FcBF_4$) redox couple was examined as a model chemistry for non-aqueous redox flow battery research. Its properties were fully characterised using voltammetry, flow-cell battery cycling, and UV-vis spectroscopy to validate flow-cell performance. Fc demonstrates facile kinetics and high stability of its oxidation states, making the $Fc/FcBF_4$ redox couple a useful low-cost model chemistry, despite its limited 0.16 M solubility in acetonitrile. By use of 'single redox couple cycling', in which only the $Fc/FcBF_4$ redox couple is battery cycled, the high capacity retention of Fc at

10 mM concentration was demonstrated; 80 % capacity retention after 200 cycles (7.8 days). The mechanism for the capacity loss was investigated and diagnosed to occur via $FcBF_4$ decomposition in the electrolyte, which proceeds irrespective of battery cycling.

1 Introduction

Redox flow batteries (RFBs) are an already established energy storage technology uniquely suited for renewable energy storage and grid-scale energy management due to their decoupled capacity and power [1]. Utilisation of entirely solution-phase redox materials avoids electron transfer reactions which are accompanied by phase changes, such as electrode deposition or intercalation, hence the battery capacity (electrolyte volume) is not dependent on the geometric electrode area (battery power output) and can be independently scaled [2]. As such, RFBs are versatile devices that can be manufactured to any desired scale and for various applications. Indeed, the state-of-art vanadium RFB (VRFB) has been successfully commercialised and demonstrated at scales upwards of 15 MW/60 MWh [3]. Although the VRFB is becoming more widely implemented, techno-economic limitations still remain relating to the relatively low energy density (~33 W h L^{-1} [4]) and high energy storage cost (~300 £ kW^{-1} h^{-1} [5]), despite VRFB chemistry being fully developed and optimised.

An intrinsic advantage of RFB technology is that the battery architecture (electrolyte reservoirs, pumps, flow cell stacks and electrode/membrane assemblies) can be easily adapted to accommodate a plethora of possible redox materials and electrolytes. This means the replacement of vanadium electrolytes with alternative energy storage materials

can, in theory, advance the technology by simultaneously increasing the volumetric capacity and decreasing electrolyte cost. One such ideology is the substitution of the aqueous electrolyte with a more electrochemically stable non-aqueous (NA) solvent [6]. Specifically, the energy density of aqueous RFBs is intrinsically limited by the small stability region of water (ca. 1.6 V in practice) which limits the RFB cell potential, if solvent decomposition is to be avoided [7]. In contrast, solvents such as acetonitrile (MeCN) are stable over 4 V [8] and have allowed NA RFBs to possess cell potentials approaching Li-ion battery technology (> 3 V) [9]. The application of NA electrolytes also offers a larger design space for redox material exploration and development such that many redox materials which are incompatible with water can be applied. Numerous metal-coordination compounds (MCCs) [10] and redox-active organic molecules (ROMs) [11] have been applied thus far and have demonstrated excellent properties. Most noteworthy, several symmetric NA RFBs based upon MCCs [12–20] and ROMs [21–25] have been demonstrated which mitigate crossover limitations, akin to the VRFB.

Although progress has been made in the NA RFB field, capacity loss in battery experiments has been observed in practically all studies and remains a significant challenge. Despite this, the cause of capacity-loss in novel systems is infrequently studied or formally identified, but often attributed to chemical instability of the redox materials. Although this conclusion is well justified in certain studies, the lack of investigation in others makes it challenging to critically assess the stability of proposed redox materials. Indeed, few efforts have been made to separate capacity fade into the contributions from chemical degradation and physical processes, such as membrane crossover or electrolyte imbalance. It is perhaps

for these reasons why few model chemistries have been proposed or fully characterised for NA RFB research thus far.

The vanadium tris-acetylacetonate system, first proposed by Liu et al. in 2009 [16], is perhaps the most widely adopted NA RFB chemistry to date due to its 2.2 V cell potential and relatively high ≈1 M solubility in MeCN [16,26–32]. Despite this, $V(acac)_3$ is a poor model chemistry with rapid capacity loss and low coulombic efficiency (≤ 90 %) [31]. In addition, the battery cycling of this compound has been inconsistent between studies with unsymmetrical charge/discharge curves, extreme potential thresholds ($0\ V \geq V_{cell} \geq 4.5\ V$ [16]) and multiple charge/discharge plateaus during cycling [16,26,27,30] being reported. The capacity loss mechanism was diagnosed to result from degradation of $V(acac)_3$ to redox active vanadyl acetylacetonate and free acetylacetone products [27], however these studies highlight the need for fully-characterised robust model chemistries in NA flow-cell testing.

More noteworthy model chemistries include 4-acetamido-2,2,6,6-tetramethylpiperidine-1-oxyl (AcNH-TEMPO) and N-(ferrocenylmethyl)-N,N-dimethyl-N-ethylammonium bis(trifluoromethane)sulfonimide ([Fc1N112](TFSI)), which were explored by Milshtein et al. in 2016 [33] and 2017 [34] respectively. In the case of AcNH-TEMPO the redox couple was used for charge-discharge studies in single redox couple experiments over relatively short timescales (25 cycles) and in cell characterisation studies via single electrolyte experiments in propylene carbonate (PC) solvent [33]. In contrast, the $Fc1N112^+$ model redox couple was developed as a higher solubility ferrocene derivative [34–36]. Here, $Fc1N112^+$ was used for flow-cell characterisation in single electrolyte experiments to study the origins of cell resistances as a function of electrolyte conductivity (MeCN vs PC) and electrode/membrane configurations [34]. Previous work by Wei, Cosimbescu et al. demonstrated the high

cyclability of $Fc1N112^+$ via charge-discharge experiments in hybrid Li-RFBs and explored its solubility in different carbonate solvents [35,36]. Nevertheless the simple ferrocene/ferrocenium ion redox couple ($Fc/FcBF_4$) and its derivatives have not yet been fully characterised despite being applied in a NA RFBs [34–39]. Indeed, capacity loss has been observed in several novel RFBs employing Fc derivatives as a posolyte, however the mechanisms have not been fully examined. To address this apparent shortcoming, we critically evaluate the suitability of the $Fc/FcBF_4$ redox couple as a model chemistry for NA RFB research and characterise its battery performance in flow-cell experiments. Here we conduct battery experiments in an 'single redox couple configuration', as shown in Figure 1a, whereby a Fc 'negolyte' (the electrolyte containing the redox couple or species with the more negative redox potential) is paired with a complimentary $FcBF_4$ 'posolyte'. Therefore, the flow-cell is 'charged' and 'discharged' by synergistically oxidising/reducing the $Fc/FcBF_4$ electrolytes respectively. Such an electrolyte configuration decreases the complexity of the system as only one redox material and two oxidation states are present in the battery [33,34,40–42]. This means the capacity retention and cycling performance of the $Fc/FcBF_4$ redox couple can be directly examined without the complication of additional redox materials or oxidation states. We investigate the origin of observed capacity loss of the $Fc/FcBF_4$ flow-cell by systematically examining plausible physical and chemical processes. The present work is therefore intended as a valuable reference material for non-aqueous flow-cell design validation and performance testing. Readers should note however that the applied single redox couple configuration is strictly speaking not a battery, as the flow-cell cannot deliver power, but rather an alternative model system. In addition, we avoid the terminology 'symmetric configuration' used in the literature [33,34,40–43] to describe the

single redox couple configuration as to avoid confusion with conventional symmetric RFBs such as the VRFB.

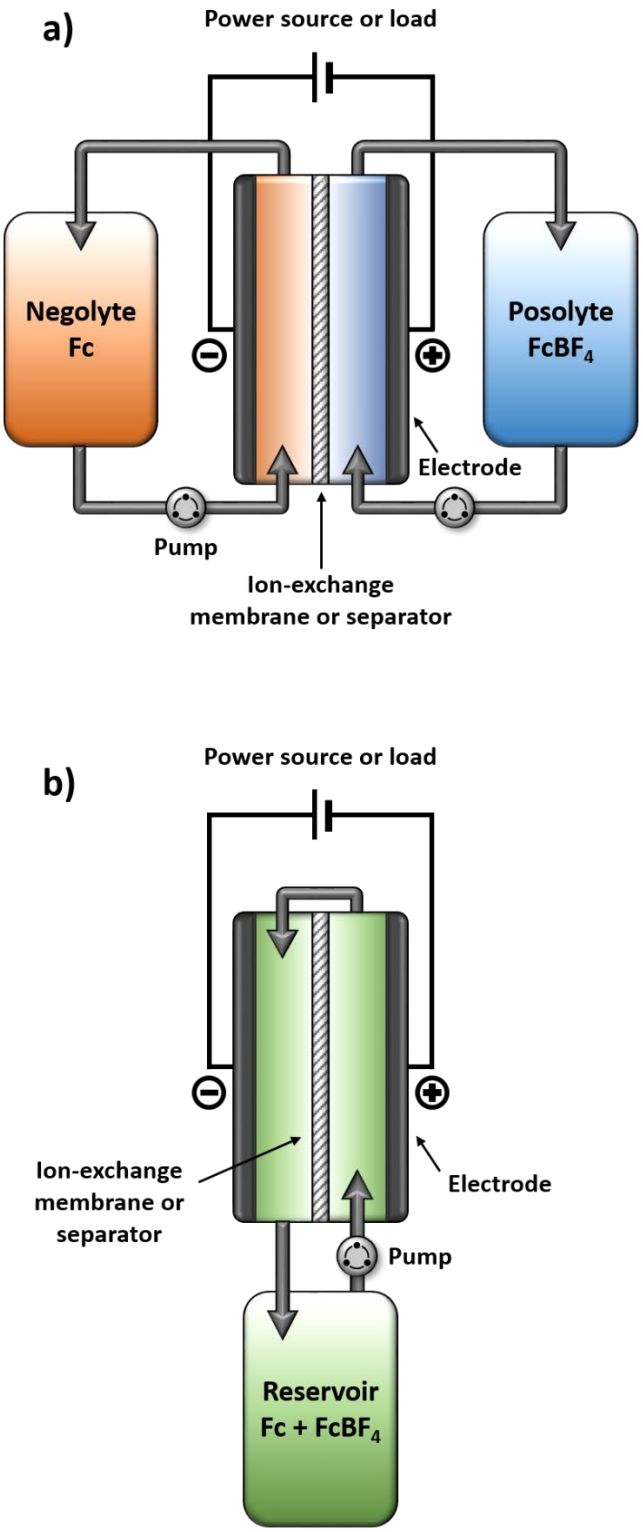

Figure 1. Schematic illustration of a redox flow battery employing $Fc/FcBF_4$ assembled in a) single redox couple configuration and b) steady-state configuration.

2 Experimental

2.1 Chemicals and materials

TEA BF_4, (Alfa Aesar 99 %), para-benzoquinone (*p*-BQ, Acros Organics 99 %), tetrafluoroboric acid solution (HBF_4, Alfa Aesar ca 50 % w/w aq. Soln.), diethyl ether (Et_2O, Fisher reagent grade), MeCN (Acros Organics 99.9 % Extra Dry over molecular sieves, Acroseal®) were purchased and used as received. Fc (98 %, Sigma Aldrich) was purified by vacuum sublimation to remove any cyclopentadiene impurity prior to usage. All other compounds were used without purification.

2.2 Ferrocenium tetrafluoroborate synthesis

$FcBF_4$ used in this work was synthesised as per literature procedures [44]. In a typical procedure, pre-purified Fc (1.01 g, 5.43 mmol) was dissolved in 30 ml Et_2O and added dropwise to a 60 ml Et_2O solution of *p*-BQ (1.17 g, 10.86 mmol) and HBF_4 50 % acid solution (3.82 g, 21.72 mmol). The resulting dark blue precipitate was filtered by Büchner filtration under vacuum and washed with 100 ml of Et_2O. The dark blue $FcBF_4$ powder was then dried under high vacuum at 60 °C and flushed with argon for storage, (1.36 g, 4.99 mmol, 91.8 %). ^1H NMR (CH_3CN, 400 MHz): δ = 33.80 ppm. Anal calcd. for $FeC_{10}H_{10}$: C 43.97, H 3.69 %; found: C 42.98, H 3.58 %.

2.3 UV-vis and solubility measurements

The spectra of Fc and $FcBF_4$ solutions in MeCN solvent were recorded at an Agilent Cary 60 spectrophotometer using either a 1 or 10 mm path length anaerobic cuvettes (Starna scientific). The solubilities of sublimed Fc and synthesised $FcBF_4$ were measured by a UV-vis method by first acquiring calibration spectra of Fc and $FcBF_4$ at 0.2, 0.4, 0.6, 0.8 and 1.0 mM concentrations in MeCN that were prepared by series dilutions of 1 mM solutions in 50 mL

volumetric flasks. Beer-Lambert calibration plots were then produced based upon the absorbance of Fc (λ_{max} = 325 and 440 nm) and $FcBF_4$ (λ_{max} = 616 nm) at UV-vis peaks. A saturated solution of each oxidation state was then prepared by making a suspension of ~1 g of solid in a small quantity of MeCN (5 mL for Fc and 2 mL for $FcBF_4$) and stirring/sonicating. The solutions were then allowed to settle for at least 30 mins and then 0.5 mL of each solution was collected, and series diluted into the calibration range. UV-vis decomposition studies were conducted by preparing 1 or 0.9 mM solutions of Fc and $FcBF_4$ in MeCN and then taking spectra every 24 h for up to 11 days. The cuvettes were stored in a N_2 glovebox between spectra to ensure anaerobic conditions. All manipulations of the $FcBF_4$ solutions were performed in a N_2 glovebox and spectra were recorded within 1 hour of preparing solutions.

2.4 Electrolyte preparation

All experiments were conducted on NA electrolytes composed of Fc and/or $FcBF_4$ redox material and TEA BF_4 as supporting electrolyte salt. Electrolytes used for voltammetry contained either 10 mM of Fc or $FcBF_4$ whereas battery cycling experiments utilised a single electrolyte in both half-cells containing 5 mM of both Fc and $FcBF_4$. Supporting electrolyte concentration was kept at a constant 0.1 M for all experiments. To generate dry electrolyte, solutions were prepared within a nitrogen glovebox (O_2 and $H_2O \leq 1$ ppm) using anhydrous solvents and vacuum dried compounds. Sublimation-purified Fc was used for all experiments and flushed with nitrogen before use. The hygroscopic TEA BF_4 salt was dried in a vacuum oven at 100 °C for at least 1 day before use. All manipulations of the air-sensitive $FcBF_4$ species in solution were conducted under anaerobic conditions.

2.5 Voltammetry techniques

Cyclic voltammograms were recorded at a glassy carbon (GC) working electrode (3 mm diameter, BASinc) using a standard 20 ml three-electrode voltammetry cell (BASinc). Rotating disk electrode linear sweep voltammograms (RDE LSVs) were conducted using an RRDE-3A apparatus (ALS Co.), 60 ml voltammetry cell and a 3 mm GC working electrode (ALS Co.). A platinum wire (BASinc) served as a counter electrode whereas a silver wire in a CoralPor-fritted glass tube (BASinc) containing supporting electrolyte (0.1 M TEA BF_4) served as a quasi-reference electrode. All experiments on Fc electrolytes were conducted under a blanket of sparging argon gas and data was recorded using either an EmStat^{3+} (Palmsens) or PGSTAT204 (Metrohm). Electrode potentials are reported versus the Fc/$FcBF_4$ redox couple. Voltammetry of $FcBF_4$ containing electrolytes was performed inside a N_2 glovebox, including RDE studies.

2.6 Battery methods

Battery experiments in a glass cell were performed using a conventional H-type glass cell (supplementary information). Charge-discharge studies were performed using 5 mL of electrolyte per half-cell with stirring. A high-porosity glass frit served as the separator whereas RVC foam served as the electrodes. For cell resistance studies, linear glass cells with either a glass frit or membrane were used. Electrochemical impedance spectroscopy (EIS) was performed as a function of electrode separation and membrane configuration using 4 mL electrolyte per half-cell without stirring. A GC macroelectrode (3 mm diameter) was inserted into each half-cell laterally such that the electrode surfaces opposed each other directly. EIS was then conducted at the 0 V cell potential with a 10 mV amplitude from 2 MHz to 1 Hz.

A conventional zero-gap flow-cell (SI) with flow-through flow fields was employed for flow-cell experiments [45]. A single 1 mm thick piece of carbon paper (Technical fibre products Ltd. 20301A, PVA binder) served as the electrode material whereas a single piece of microporous separator (Celgard® 2500; 25 µm microporous monolayer, 55 % porosity) served as the membrane. Polarization curves and EIS data were recorded with the flow-cell assembled in a steady-state configuration with 10 mL of electrolyte at 50 % state-of-charge at different flow rates [34]. EIS was conducted at the 0 V cell potential with a 10 mV amplitude from 200 kHz to 5 mHz. Charge-discharge studies were performed with the cell in a single redox couple configuration which was pumped at a flow rate of 10 ml min^{-1}. Applied currents increased in increments of 5 mA, which were converted to corresponding current densities by use of the electrode geometric area of 2.08 cm^2.

Galvanostatic and potentiostatic experiments were recorded using either a PGSTAT204 (Metrohm) or Compactstat (IVIUM) with a temporal resolution of ≤2 s. For polarization studies, a chronoamperometry method was used with 300 s potential holds in 50/100 mV increments from 0 to 1 V. The current and potential responses were then averaged across each 300 s step to give single I-V datapoints as a function of flow-rate.

3 Results and Discussion

Fc is an organometallic compound consisting of an Fe(II) core coordinated to two cyclopentadienyl ligands, which undergoes reversible oxidation to the stable Fc^+ ion. The oxidation of Fc to Fc^+ is a classical and well understood reversible one-electron redox process which involves the removal of an electron from the stable 18e d^6 Fe(II) electronic configuration to the 17e d^5 Fe(III) species [46]. The kinetics of this process are known to be fast because the Fc and Fc^+ geometries are almost identical; an Fe-C bond lengthening of

only 0.1 Å occurs upon oxidation [46]. In addition, the electrochemistry of Fc is known to be mostly unaffected by variations in solvation (it is an internal referencing standard for reporting potentials in NA electrolytes) [47], thus allowing Fc to be used in many possible electrolytes. As such, Fc displays several characteristics desirable for applications in RFBs whereby an ideal model chemistry would fulfil several criteria;

- Indefinite stability of all accessed oxidation states in both solid and solution phase
- Commercial availability of each oxidation state *or* a method to prepare them via convenient synthesis
- High solubility of each oxidation state in various electrolytes in order to avoid precipitation under different battery conditions
- Good electrochemical properties such as fast redox kinetics and high diffusion coefficients
- A significant potential separation from the onset of electrolyte decomposition or parasitic reactions to allow for unrestricted battery cycling
- Low material cost, low toxicity and ease of handling

In this regard, the Fc/Fc^+ redox couple is an attractive model chemistry because both Fc and $FcBF_4$ are low-cost commercially available products which are relatively low toxicity. In the present work however, the $FcBF_4$ material was synthetically prepared by chemical oxidation of Fc via a simple and inexpensive one-step reaction that gives the $FcBF_4$ product as a pure precipitate (92 % yield). The product was found to be an air- and light-stable dark blue powder that could be stored under ambient conditions for several months without observed decomposition, as reported by other groups [44]. We report the maximal solubilities of Fc and $FcBF_4$ in pure MeCN as 0.16 and 1.20 M respectively which are

consistent with other reports [34–36,48]. The solubility of the material is therefore limited by the Fc oxidation state which is an order of magnitude lower than $FcBF_4$ due to its low polarity. This therefore restricts the battery application to concentrations of up to ~0.1 M if Fc precipitation is to be avoided. Indeed, the low solubility of Fc in conventional battery solvents is a well-known issue in the literature, however efforts to increase its solubility for practical application have been successful, with $Fc1N112^+$ being soluble up to 1.7 M in carbonate mixtures [36]. In the present work, battery cycling using the $Fc/FcBF_4$ redox couple was performed at a diluted concentration of 10 mM Fc which is sufficient for flow-cell testing and validation.

3.1 Characterisation of the $Fc/FcBF_4$ redox couple

The reversible oxidation of Fc to the Fc^+ ion presents as a classical one-electron diffusion-limited redox couple when probed by cyclic voltammetry (Figure 2a). This is best characterised as quasi-reversible however because the peak separation is relatively large and increases with scan rate (Figure S5). Indeed, at a slow scan rate of 10 mV s^{-1} a large 100 mV separation is observed as compared to the theoretical 59 mV separation for a fully reversible redox couple. Despite this, the Fc/Fc^+ voltammogram is highly symmetric and gives peak current ratios close to unity (0.98 to 1.08) at all scan rates, which demonstrates the high stability of both the Fc and Fc^+ oxidation states on a voltammetry timescale. By use of Randles-Sevcik analysis at low scan-rates (≤100 mV s^{-1}) we report a high Fc diffusion coefficient of 2.10×10^{-5} cm^2 s^{-1} which is consistent with other reports [48]. In addition, we report a relatively high standard electrochemical rate constant of 2.40×10^{-2} cm s^{-1} by use of Koutecký-Levich analysis at an RDE (SI), which indicates desirably facile kinetics at carbon-based electrodes.

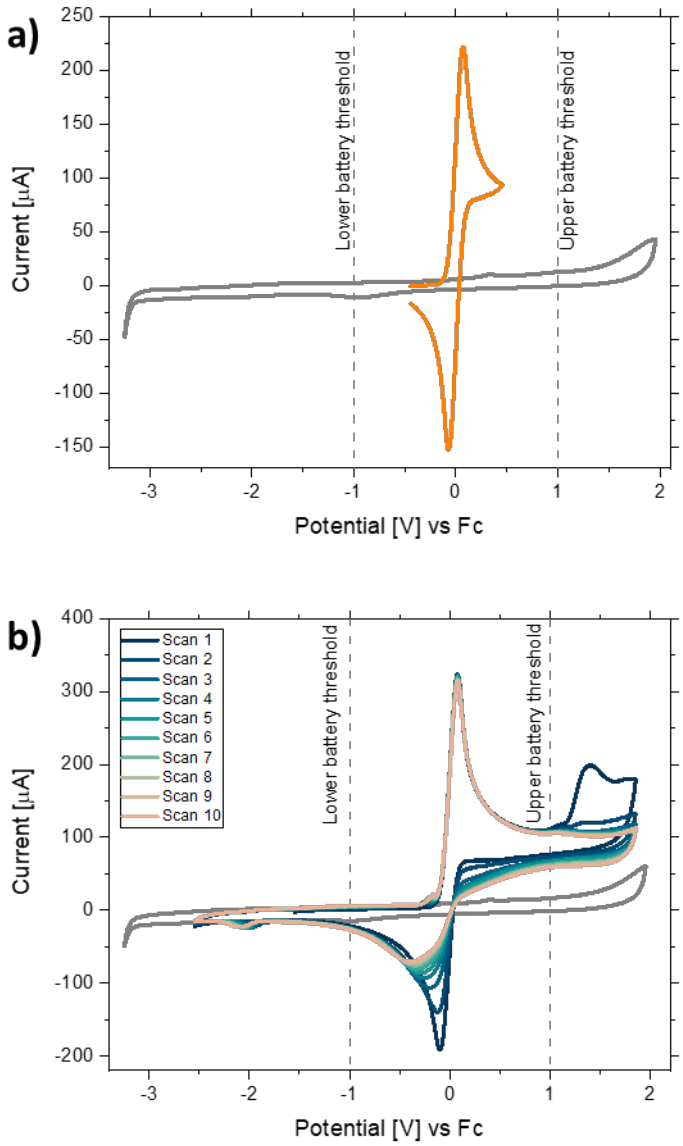

Figure 2. Cyclic voltammetry of 10 mM Fc in 0.1 M TEA BF_4, MeCN. Blank voltammetry of the supporting electrolyte is given in grey and vertical dashed lines represent the upper and lower battery potential thresholds at ±1 V. a) Fc redox potential in comparison to the supporting electrolyte (50 mV s^{-1}). b) CV of Fc in a wider potential range. 10 scans shown (100 mV s^{-1}).

A desirable property for RFB redox materials is the electrochemical inertness of the material at other potentials so as to avoid parasitic processes occurring within the battery in the case of membrane crossover or high overpotentials occurring. Here the Fc electrolyte is

inert at cathodic potentials in the range of -3 to 0 V vs Fc, however a second oxidative process occurs at approximately 1.5 V vs Fc (Figure 2b) which corresponds to the formation of an unstable dication [49]. The decomposition of this species was observed to affect the reversibility of the $Fc/FcBF_4$ redox couple such that the Fc^+ back-reduction peak became increasingly broad and shifted negatively with scan number, which is consistent with a decrease in redox kinetics. This behaviour was attributed to electrode fouling of decomposed material resulting from the irreversible $FcBF_4$ oxidation, which was visibly observed on the electrode. Interestingly, the forward Fc oxidation peak remained mostly unaffected by the fouling (a small loss in current response), which suggests that the Fc oxidation mechanism is invariant of the electrode surface structure. To ensure that the $Fc/FcBF_4$ redox couple does not form an electrode film with cycling, thus affecting its own redox kinetics, 100 consecutive scans were conducted in a narrow -0.4 to 0.4 V vs Fc potential region (Figure S4). No change in reversibility or decrease in current response or was observed, thus indicating high cyclability of Fc.

In principal the irreversible ferrocenium oxidation is problematic for RFB application as it would simultaneously cause passivation of the electrode and capacity loss during cycling, however, as shown in Figure 2b, a large battery overpotential of >1 V would be required to initiate dication formation. Indeed, as the $Fc/FcBF_4$ redox couple resides roughly central in the electrolyte stability region, a battery employing $Fc/FcBF_4$ can be cycled with large overpotentials of ±1 V without incurring unwanted decomposition of the supporting electrolyte or $FcBF_4$ species. These large battery thresholds therefore do not restrict the battery potential when overpotentials manifest at high current densities.

3.2 Electrochemical impedance spectroscopy and polarisation

By use of the Fc/$FcBF_4$ redox couple, flow-cell performance can be examined under practical and realistic operating conditions. First, by assembly of the flow-cell in a 'steady-state configuration' (Figure 1b) [43], whereby one electrolyte at 50 % state-of-charge (SOC) is cyclically pumped through both half-cells, the flow-cell area-specific resistance (ASR) can be quantified [34]. Here a reference electrode is not required because similar processes occur at both electrodes. In addition, as the electrolyte composition remains constant, cell-level polarization and EIS can be conducted at steady-state giving reliable measurements of cell resistances and IV-characteristics [34]. The EIS Nyquist plots of the flow-cell as a function of flow-rate are shown in Figure 3a. Considering the EIS waveform, for each flow-rate two semicircles and a Z' intercept was observed. Whereas the diameter of the first semicircle is invariant of flow-rate, the second decreases in size as flow-rate increases and can be attributed to mass-transport. Therefore, the EIS data can be rationalised as the sum of ohmic (R_Ω) , charge-transfer (R_{CT}) and mass-transfer (R_{MT}) resistances, corresponding to the x-intercept, semicircle one and two respectively. Analysis of the EIS data gives an ohmic resistance of 5.68 Ω (11.81 Ω cm^2), whereas the charge-transfer resistance was a considerably smaller contribution of only 0.98 Ω (2.04 Ω cm^2), which can be attributed to the fast kinetics of the Fc/$FcBF_4$ redox couple. The large ohmic resistance was attributed to the low electrolyte conductivity and membrane resistance, however the ohmic resistance here is reasonable given that the supporting electrolyte concentration is only 0.1 M. For comparison, a R_Ω of ≈2 Ω cm^2 was reported by Milshtein et al [34] for a flow-cell utilising a Daramic separator and 1 M $Fc1N112^+$, 0.5 M TEA TFSI, MeCN electrolyte.

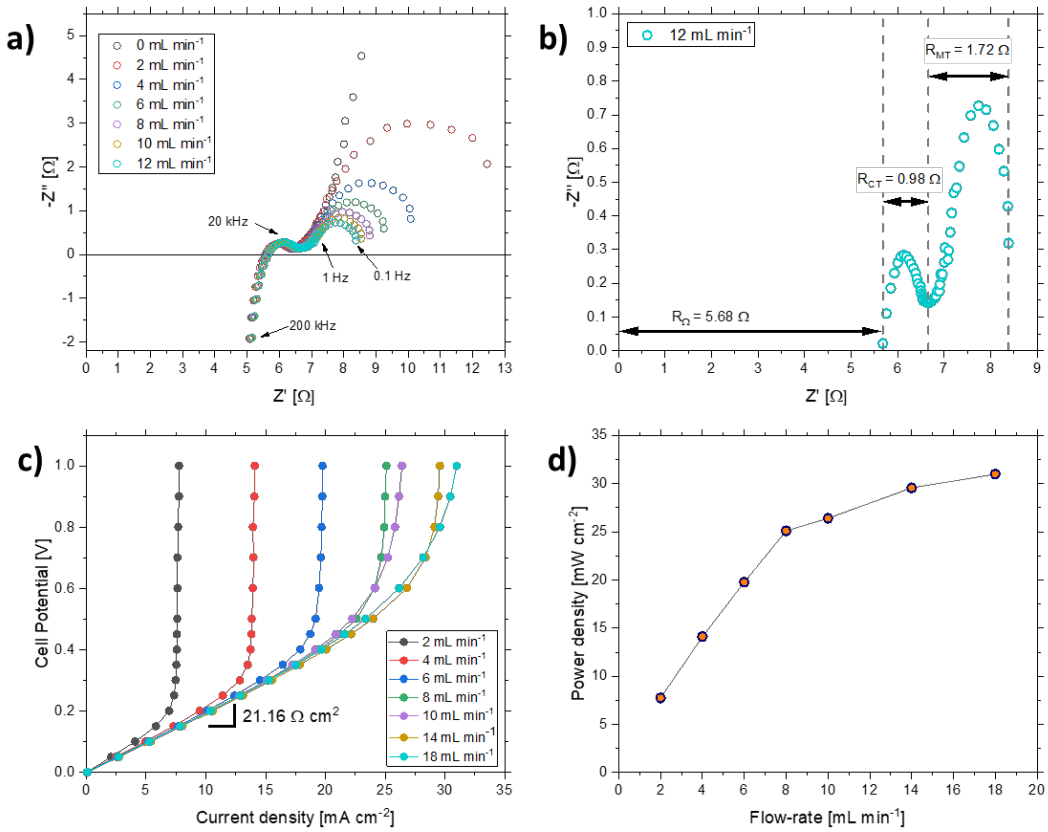

Figure 3. a) Electrochemical impedance as a function of flow-rate. b) analysis of the EIS spectrum of the flow-cell at 12 mL min^{-1}. The ohmic resistance (R_Ω), charge-transfer resistance (R_{CT}) and mass transport resistance (R_{MT}) are shown. c) Polarization curves as a function of flow-rate. d) Maximum power density (at 1 V cell potential) as a function of flow-rate.

The polarization curves in Figure 3c give the cell potential as a function of current density for various flow-rates, allowing the cell resistance to be interpreted under different operating conditions. For each curve a linear relationship at low overpotentials is observed which gives a resistance equivalent to the flow-cell ASR; 21.16 Ω cm^2 [33]. This gradient was observed to decrease slightly as the flow-rate increased which indicates that the cell ASR decreases due to enhanced reactant transport to the porous electrodes (Figure 3c). At high overpotentials the polarization curves become vertical indicating significant increases in cell

resistance. This behaviour was rationalised as the point where the flow-cell depleted the redox species via full conversion, thus starving the flow-cell of reactants and giving a maximum current density. This is given in Figure 3d which indicates that the power density approaches a maximum as the flow-rate is increased. An electrolyte flow-rate of 10 mL min^{-1} was adopted as the default flow-rate for battery experiments in the present work as a balance between performance and reliability.

3.3 Battery performance of the Fc/$FcBF_4$ redox couple

Galvanostatic electrolysis of the Fc/$FcBF_4$ flow-cell produces charge-discharge curves which model a full RFB as shown in Figure 4a. However, as opposite reactions of the same redox couple occur at each electrode, the cell potential is precisely 0 V; as measured by the open-circuit voltage when at 50 % SOC. Concurrently, the electrochemical interconversion of the electrolytes is accompanied by corresponding colour changes such that the solutions alternated between yellow (Fc) and dark blue ($FcBF_4$) via a green intermediate (a mixture of Fc and $FcBF_4$), as shown in Figure 4a. At a current density of 2.40 mA cm^{-2} (corresponding to a C-rate of 1.87C, see SI section 4 for the definition of battery metrics) well-defined charge-discharge plateaus were observed slightly above and below the 0 V cell potential. Corresponding overpotentials of only 58 and 60 mV respectively (calculated as averaged cell potentials) were observed, thus indicating high voltaic efficiency and good performance at moderate C-rates. In addition, the flow-cell demonstrated 100 % capacity on the first cycle (Figure 4c), thus indicating full utilisation of the Fc/$FcBF_4$ electrolytes. Thereafter the capacity retention was relatively high as the cell was continuously cycled for over 7 days and after 200 cycles (7.8 days), 80 % of the initial capacity was retained. A correspondingly high

mean coulombic efficiency of 98.5 % was recorded, which indicates high stability of the $Fc/FcBF_4$ redox material in the MeCN electrolyte.

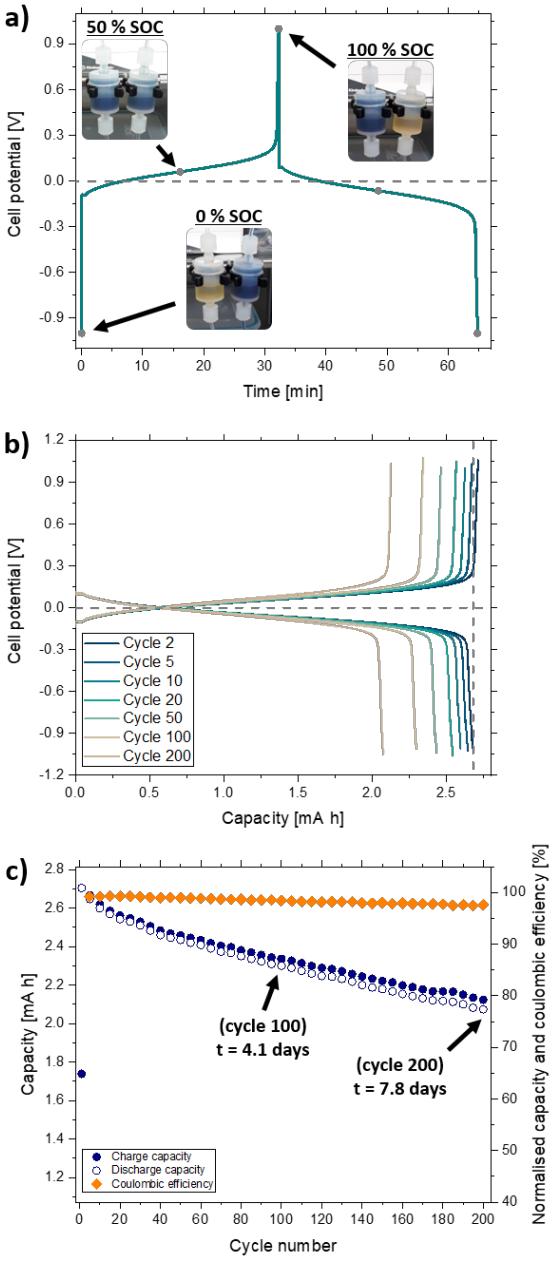

Figure 4. a) Typical charge-discharge curve of the $Fc/FcBF_4$ flow-cell. Photographs are shown of the electrolyte reservoirs at 0, 50 and 100 % SOC. b) Selected charge-discharge curves during battery cycling. The vertical dashed line indicates the 2.68 mA h cell capacity. c) Capacity and coulombic

efficiency as a function of cycle number (cell cycled from an initial SOC of 50 %). 5 mM Fc/$FcBF_4$, 0.1 M TEA BF_4, MeCN electrolyte at 10 mL min^{-1}, 2.40 mA cm^{-2} (1.87C).

Battery cycling of the flow-cell at higher current densities was conducted to examine the performance and capacity as a function of applied current (Figure 5). Here the battery overpotential increased with the applied current density, such that at 12.02 mA cm^{-2} the average potential was ±220 mV. In part, the increased overpotentials are due to ohmic losses (IR_Ω) which scale with the applied current (ca. 142 mV at 12.02 mA cm^{-2} for R_Ω = 5.68 Ω), however as shown in Figure S17 and Figure S18 whereby ohmic losses have been subtracted, additional overpotentials are present. Based on the steady-state studies, this additional overpotential can be attributed to mainly mass-transport limitation with an additional minor contribution from the reaction kinetics. More strikingly in Figure 5, the capacity of the battery also showed an inverse trend with the applied current density; Initially at 1.87C the cell achieved 100 % capacity, however at 3.73C, 5.60C, 7.46C and 9.33C, only 89, 83, 78 and 72 % was achieved respectively. This behaviour can be attributed to the finite mass transport which causes increased concentration overpotential as the applied current is increased. At higher C-rates the cell was unable to reliably cycle such that at 14.42 mA cm^{-2} and above, the battery capacity was typically <50 % and frequently inconsistent. Regardless, Figure 5b shows that high C-rates of up to ≈10C can be achieved with the Fc/$FcBF_4$ redox couple at modest flow-rates with minimal overpotential and high accessible capacities. This performance can be directly compared to charge-discharge studies in a conventional glass-cell (Figure S13) whereby considerably poorer performance was observed. Due to the large electrode separation in glass cells (∼15 mm) and the glass frit separator utilised, a significantly higher ohmic resistance of ∼18.5 Ω cm^2 was observed (SI).

In combination with the inferior glass-cell convection, the high cell resistance limits the maximum current density and yields large overpotentials (~600 mV at 1 mA current). As such, only very low C-rates of ≤0.75C could be achieved which are an order of magnitude less than in the flow-cell.

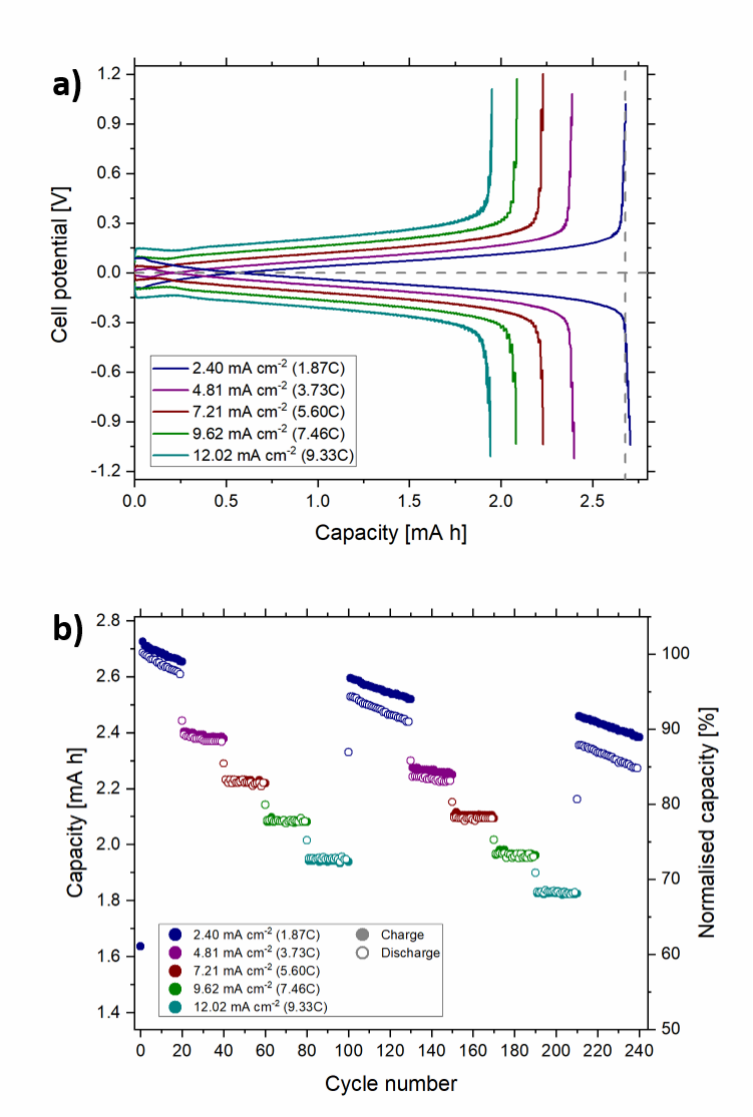

Figure 5. Battery cycling of the Fc/$FcBF_4$ redox couple in a flow-cell as a function of current density. a) An overlay of charge-discharge curves at different current densities. Cycles 2, 22, 42, 62 and 82

are shown. The vertical dashed line shows the theoretical 2.68 mA h capacity. b) Capacity and normalised capacity against cycle number. (5 mM Fc/$FcBF_4$ in 0.1 M TEA BF_4, MeCN electrolyte).

3.4 Diagnosis of capacity loss

Thus far, the Fc/$FcBF_4$ redox couple was evaluated in terms of its electrochemical performance, however as is evident in Figure 4c and Figure 5b, a significant capacity fade was observed across all battery experiments over long periods of time. The mechanism for the capacity loss was not immediately obvious as our voltammetry experiments did not show any electrolyte decomposition over relatively short timescales or specific instability within the potential thresholds accessed. Therefore, additional experiments were conducted to deduce the capacity loss mechanism by use of simple diagnostic battery methods. Generally speaking, all capacity loss in RFBs can be attributed to a loss of redox material from the electrolytes, however the mechanism for this loss can be either due to a physical or a chemical process, as shown in Figure 6. To identify the specific mechanism in the present work, we employed a methodical approach by process of elimination, as summarised in Figure 7.

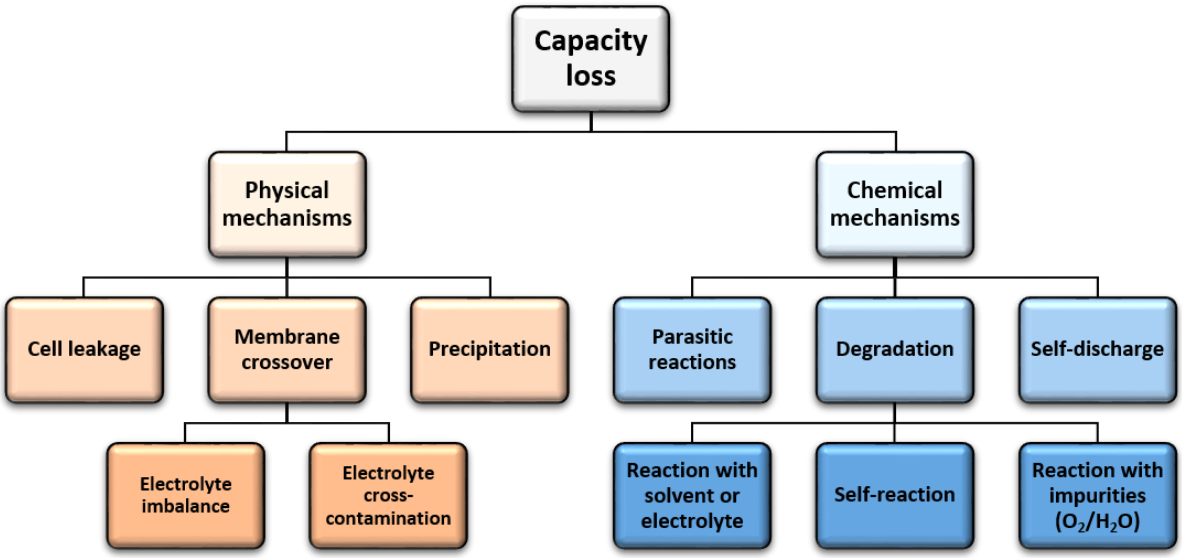

Figure 6. Characteristic capacity loss mechanisms in RFBs.

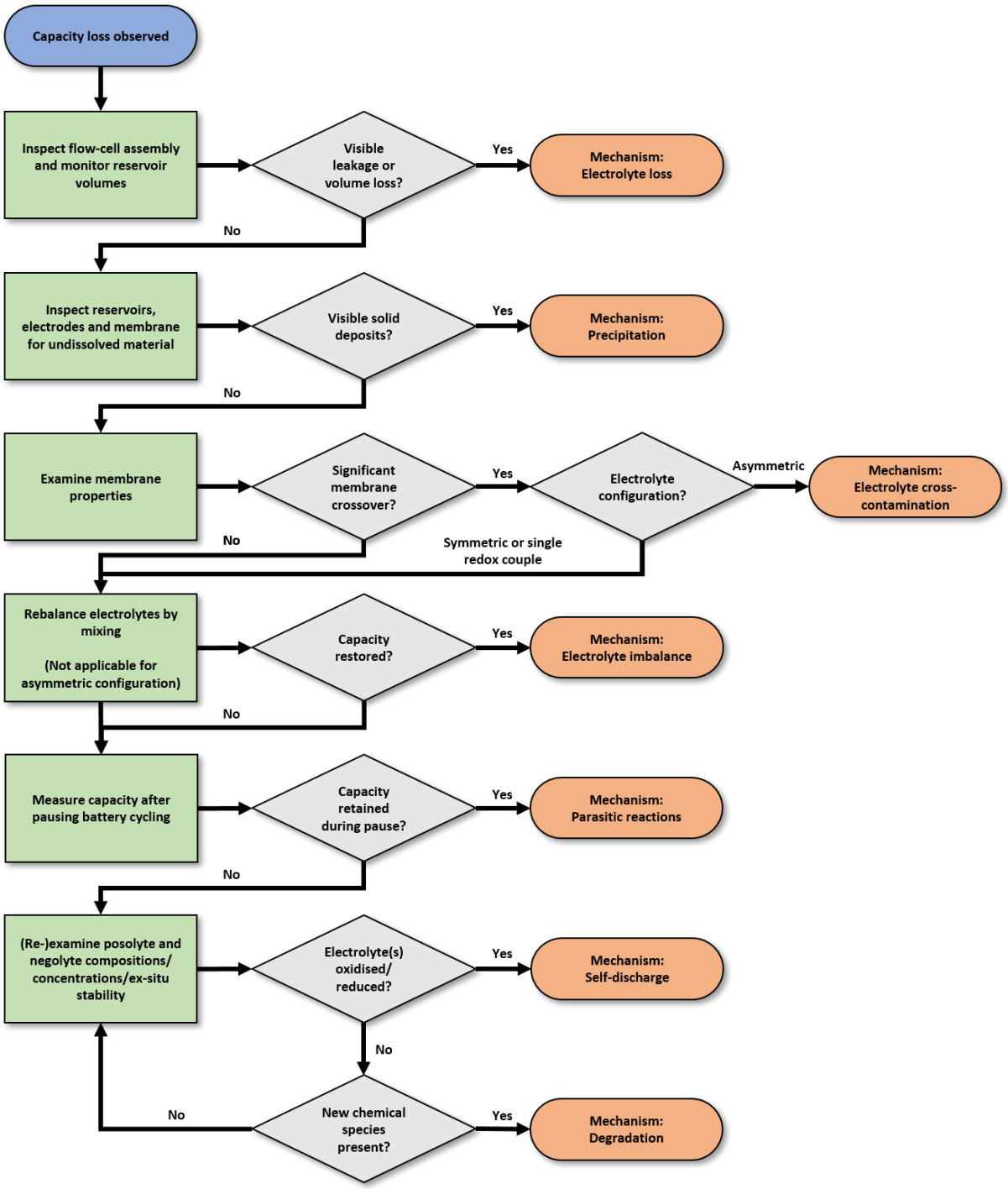

Figure 7. Methodology flowchart for diagnosing capacity loss in RFB experiments. Readers should note that capacity loss mechanisms are not mutually exclusive because multiple mechanisms may contribute to the observed capacity fade.

Firstly, the flow-cell was examined post-cycling to observe any electrolyte loss due to cell leakage. It is challenging to prevent all leakage from NA flow-cells because organic solvents present unique chemical compatibility issues, thus making NA flow-cell design problematic from an engineering perspective. Most significantly, solvents such as MeCN are relatively non-polar and therefore poorly repelled by conventional gasket materials. Indeed, we have observed a tendency for NA electrolytes to diffuse through/between gaskets and evaporate off solvent, as noted by others [50]. This process slowly decreases the solvent volume and leaves behind crystalline formations on the gasket edges composed of the redox materials and supporting salt. Despite this, the total volume loss after 7 day battery experiments was imperceivably small and did not account for the observed capacity loss (~20 %). In addition, experiments using a preconditioned flow-cell (cyclically pumped with supporting electrolyte only for 24 h) yielded no improved capacity retention, thus eliminating the possibility for capacity loss due to electrolyte soaking into the cell architecture. This conclusion is also supported by the observed capacity loss in glass-cell cycling experiments (Figure S13) in which electrolyte leakage is impossible.

Capacity loss due to the poor selectivity of the porous separator was then investigated to exclude the possibility of crossover-induced capacity loss. As only one redox couple was used in cycling experiments here, membrane crossover cannot cross-contaminate the electrolytes, however it is possible that unequal pressure on the separator could force an electrolyte imbalance. This can cause the concentrations of Fc/$FcBF_4$ or the total volume of electrolytes to become non-equal, thus causing the capacity to be limited by one half-cell. To examine this, the electrolytes were rebalanced midway through cycling as shown in Figure 7a. Here, rebalancing of the electrolytes did not restore the cell to the initial capacity

which indicates that the flow-cell remained balanced in our experiments. The observed capacity loss was therefore attributed to either chemical or electrochemical processes occurring in the battery, such as parasitic reactions or degradation of the $Fc/FcBF_4$ redox material. Parasitic reactions, such as H_2 evolution in the VRFB, compete with the intended electrochemical processes in the RFB and typically cause capacity loss with time via cell imbalance. Here we identify no such reactions because the battery electrolyte is inert within the ±1 V potential limits (Figure 2a) and moreover the capacity loss occurs irrespective of applied currents. As shown in Figure 8b the capacity decreased linearly with time which indicates that the capacity loss is most likely due to a slow chemical reaction which occurs in the electrolyte. Furthermore, this experiment proves that the capacity loss has a time-dependency rather than a cycle number dependency which is typical in other battery technologies [51]. This time dependency is most obvious in Figure 5 whereby the capacity loss rate is fastest at 2.40 mA cm^{-2} (3.31×10^{-3} mA h $cycle^{-1}$) and slowest at 12.0 mA cm^{-2} (8.46×10^{-5} mA h $cycle^{-1}$) because the time taken to complete a cycle decreases as the current density increases. In fact, the overriding capacity loss in Figure 5 showed a linear relationship with time, giving a near-constant loss rate per hour at all current densities of 1.07×10^{-2} C h^{-1}.

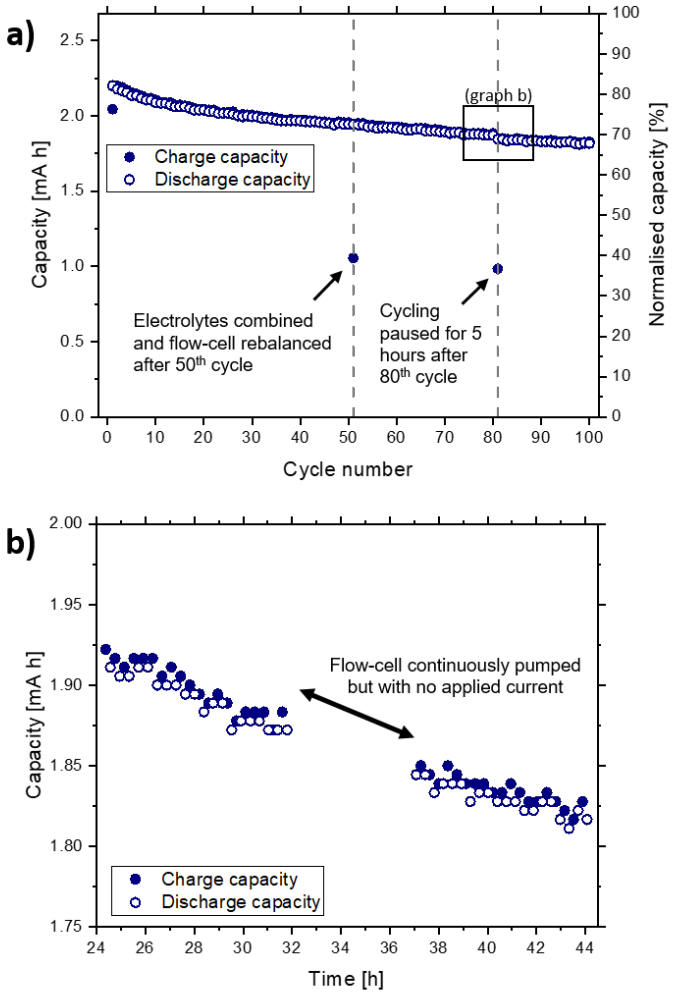

Figure 8. Capacity loss study of the Fc/$FcBF_4$ system in the NA flow-cell. a) capacity vs cycle number. The battery electrolytes were recombined and rebalanced at the 50th cycle whereas the cell cycling was paused for 5 h at the 80th. b) capacity vs time during the cycling pause (cycle time defined by the start of each charge/discharge step). 5 mM Fc/FcBF4, 0.1 M TEA BF_4, MeCN electrolyte at 10 mL min^{-1}, 4.81 mA cm^{-2} (3.73C).

Given that the neutral Fc oxidation state is known to be exceptionally stable [46], it was suspected that decomposition of Fc^+ was the likely reaction. This was confirmed by conducting UV-vis analysis of each oxidation state in anaerobic MeCN solution at 1 mM concentration. While the Fc solution showed no change after 15 days (Figure S2), the $FcBF_4$

solution showed considerable evolution of the UV-vis spectrum as shown in Figure 9b, with the largest change occurring over the first 24 h. In addition, the instability of $FcBF_4$ was visually observed in solutions of MeCN electrolyte; solutions of $FcBF_4$ in only MeCN gave a deep blue colour that persisted for at least one week, whereas solutions of $FcBF_4$ with TEA BF_4 supporting salt were more blue-green in appearance and after several days they were pale-green. This observation was also seen in the battery experiments where the combined $Fc/FcBF_4$ green electrolyte appeared greener and more transparent after 7 days of cycling, indicating a loss of the $FcBF_4$ species. The instability of $FcBF_4$ in organic electrolytes is well known in the literature [52–54] as the Fc^+ ion is an oxidising agent and in particular, it rapidly decomposes in the presence of oxygen as shown in Figure 9a, to give iron oxide and cyclopentadienyl-decomposition products [53–55]. In the present work, the battery electrolytes were maintained in an anaerobic N_2 glovebox with oxygen levels at 1 ppm maximum which excluded oxygen from the experiment. Furthermore, the addition of an antioxidant, 2,6-diterbutyl-4-methyl phenol at 1 mM concentration [53], failed to improve the $FcBF_4$ stability as the UV-vis spectrum showed similar evolution with time as the control. The effect of trace water in the battery electrolyte was also examined to ensure that $FcBF_4$ is not water-reactive. UV-vis experiments were conducted in anaerobic conditions with varying quantities of water (0.56 M to 2.78 M), however the decomposition rate was equal to the control (Figure S3). Thus, $FcBF_4$ is not directly reactive towards water because the water content was in very large excess, and in addition, $FcBF_4$ has been routinely manipulated in aqueous solutions in the literature [44,54].

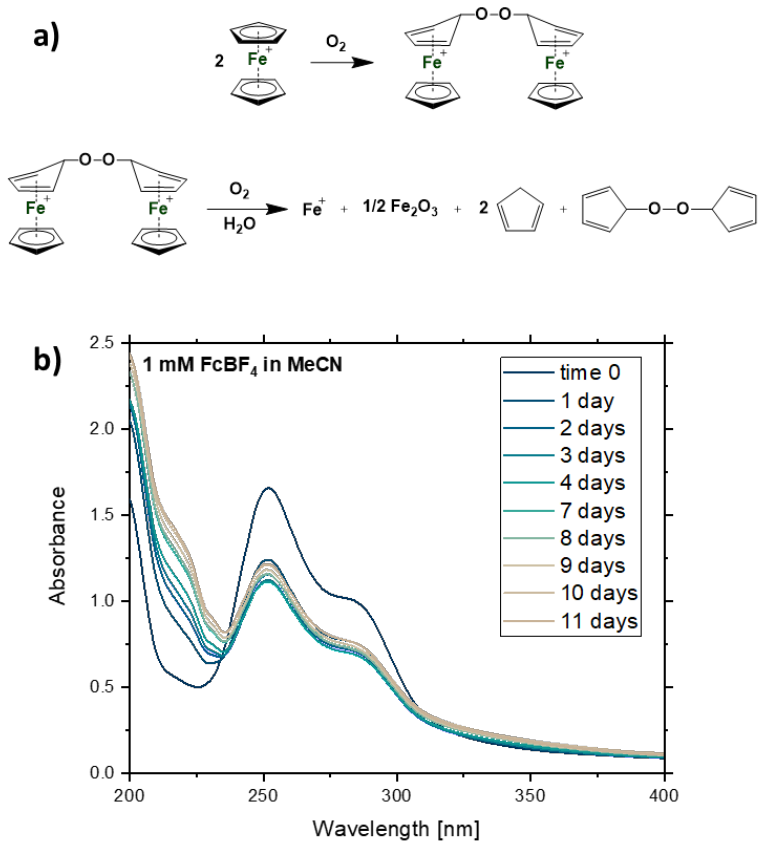

Figure 9. a) The decomposition mechanism of ferrocenium cations in the presence of oxygen [52–54]. b) The evolution with time of the UV-vis spectrum of 1 mM $FcBF_4$ in MeCN.

By eliminating possible reactions with electrolyte impurities, we conclude that $FcBF_4$ is reactive towards either the solvent or supporting salt. The precise reaction remains unclear at present; however, we observe that $FcBF_4$ can self-discharge via chemical reduction to Fc. This is most apparent in our experiments when conducting voltammetry on $FcBF_4$ electrolytes which indicates the presence of Fc in the bulk solution. For example, the anodic current response at potentials higher than the Fc/$FcBF_4$ redox potential increases with rotation rate at an RDE (Figure S10). The decomposition of $FcBF_4$ to give Fc (among other products) has been previously observed in aerobic solutions of dimethylformamide or Dimethyl sulfoxide [53], however this has not been observed previously in anaerobic MeCN

electrolytes. Despite this, we also observe a decrease in total Fc quantity (Fc + $FcBF_4$) in battery electrolytes with time (Figure 10), which indicates that the $FcBF_4$ decomposition reaction yields additional products.

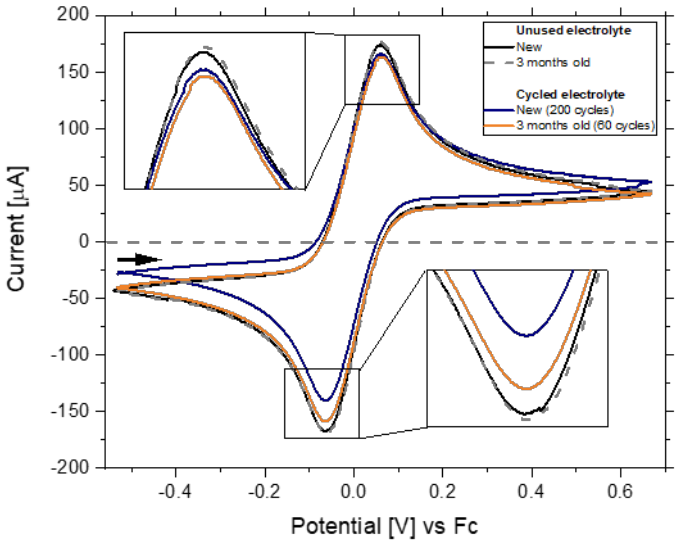

Figure 10. Cyclic voltammetry of $Fc/FcBF_4$ battery electrolytes at 50 mV s^{-1} (solutions initially prepared with 5 mM Fc and 5 mM FcBF4 in 0.1 M TEA BF4, MeCN). The current response of a freshly prepared electrolyte is compared to a three month old electrolyte, as well as electrolytes recovered from battery studies at different cycle stages.

3.5 Comparison to other NA RFB model chemistries

The $Fc/FcBF_4$ redox couple has demonstrated excellent properties as a model chemistry for the characterisation of NA flow cells. Table 1 compares the $Fc/FcBF_4$ couple to three of the other compounds that have been utilised in this manner, including the commonly used $V(acac)_3$ complex. All materials, with the exception of Fc1N112, are commercially available, the latter requiring complicated synthesis. However, it is notable that the $V(acac)_3$ species is often received in an impure form that includes the $VO(acac)_3$ species. Substantial

purification steps must be undertaken to achieve the pure $V(acac)_3$ which is essential to obtain clean voltammetry and optimal flow cell performance [56]. Furthermore, the material is only commercially available in the neutral oxidation state, thus additional synthesis is necessary to synthesise either the reduced or oxidised form, depending on the redox cycling desired. The TEMPO derivative is also commercially available, as it is routinely used in catalysing organic synthetic reactions and as a redox mediator in some Li-ion battery devices [57,58]. Fc is a low cost, readily available compound that has an established and well characterised role in electrochemistry as the typical standard reference couple for non-aqueous chemistry. It I also commercially available in both the neutral and charged state.

Table 1: Comparison of redox species used as model chemistries for NA RFBs. (a) Capacity figures and experiment times were not fully reported in the literature. The values here are calculated or estimated from the literature procedure and published results. (b) Battery cycling was only conducted between 0 and 50% SOC. (c) The total electrolyte volume was not reported and therefore the theoretical capacity is unknown.

Compound	Material availability	Solubility (solvent)	Cycles in flow cell	Discharge capacity at 10th and 100th cycle (total experiment time)[(a)]	Ref
$V(acac)_3^{-/0/+}$	Commercially available as $V(acac)_3$ only.	$V(acac)_3$ = 1 M (MeCN)	11 cycles (H-cell)	10th cycle = 5.2 mA h, 38% (~750 h)	[27,31, 55]
$V(acac)_3^{-/0/+}$	Commercially available as $V(acac)_3$ only. Extensive purification.	$V(acac)_3$ = 1 M (MeCN)	160 (operating to 50 % state of charge)	100th cycle ≈ 134 mA h, 50%[(b)]	[56]
AcNH-TEMPO$^{0/+}$	Commercially available as AcNH-TEMPO and AcNH-TEMPO$^+$	AcNH-TEMPO$^{0/+}$ ≥ 0.5 M (PC)	20	10th cycle ≈ 12 mA h, 90%	[33]
$[Fc1N112]^{+/2+}$	Must be synthesised	$[Fc1N112]^+$ = 1.7 M (EC/PC/EMC)	100	100th cycle ≈ 70 mA h[(c)]	[34,36]
$Fc/FcBF_4$	Commercially available as Fc and $FcBF_4$	Fc = 0.16 M $FcBF_4$ = 1.2 M (MeCN)	240	10th cycle = 2.64 mA h, 98.4% (10.5 h) 100th cycle = 2.33 mA h, 87.0% (44.0 h)	This work

The Fc species, in the context of this comparison, is let down by its poor solubility. While the $FcBF_4$ species attains a comparable solubility to the other materials, the Fc itself operates at an order of magnitude lower (0.16 M). Yet this is not a problem for the

characterisation of flow cells, as one would typically operate at concentrations of 10 – 50 mM as opposed to 1M.

Regarding cycle life and capacity retention the best demonstration to date in the literature was 100 cycles delivered by the ferrocene derivative, Fc1N112 [36], and 160 cycles from a purified $V(acac)_3$ system [56]. Comparison of capacity retention to these reports is difficult due to poor reporting of capacity figures (Table 1), especially in terms of the normalised capacity and total experiment time. Regardless, though at lower concentration, the Fc couple reported in this work readily achieve 240 cycles, retaining 87% capacity at 100 cycles. It is also evident that the decay is not due to cycling but a time limited decomposition of the $FcBF_4$ species. Thus, depending on the applied current and electrolyte volume, considerably more cycles could be achieved giving more impressive capacity retention.

The results presented by Saraidaridis and Monroe [56] are interesting, as most reports show $V(acac)_3$ decomposes quickly and yields multiple redox active decomposition products [27]. In addition, the upper threshold potential must be restricted when cycling $V(acac)_3$ to avoid decomposition, which causes poor cycling efficiency and complicates flow-cell diagnostics. However, reported that this was again due to $VO(acac)_3$ impurity in past studies, thus on extensive complex purification, a flow cell utilising the $V(acac)_3$ complex attained high current densities of up to 100 mA cm^{-2}. This involved only charge-discharging to 50% state of charge (SOC) however (based on the initial capacity), which is possibly why the degradation of 80% after 20 cycles predicted by Kucharyson et al. [59] is not observed. In comparison, the $Fc/FcBF_4$ cycling here was charge-discharged to full conversion on each cycle which gives more reliable capacity measurement.

4 Conclusions

The suitability of the Fc/$FcBF_4$ redox couple as a model chemistry for NA RFB research was evaluated by fully characterising its properties using voltammetry, spectroscopy and battery methods. Due to fast redox kinetics, high stability, low cost and simplicity, the Fc/$FcBF_4$ redox couple is a useful model chemistry for flow-cell validation and testing. By conducting single redox couple cycling, in which Fc oxidation is paired with $FcBF_4$ reduction in a flow-cell, the high capacity retention of the system was demonstrated with 80 % remaining after 200 cycles (>7 days). The cause of capacity loss was systematically identified to result from chemical instability of the $FcBF_4$ oxidation state, however the timescale for this process is very long and does not affect flow-cell validation and diagnostics.

The observations presented herein explain the capacity loss observed in novel NA RFBs employing Fc or Fc-derivatives which has yet to be investigated [34–39,48]. This work highlights the importance of investigating capacity loss in novel RFBs as even *simple* redox materials can display complex chemical reactivity. In addition, we demonstrate that voltammetry techniques are generally inadequate for assessing electrolyte stability due to their short timescales. As such, we recommend the flow-cell experiments applied here as more rigorous methodologies for capacity loss diagnosis, and in particular to discern losses due to both physical and chemical processes which occur in the RFB technology.

Acknowledgments

This work was funded by Lancaster University. The authors declare no conflicts of interest.

References

[1] J. Noack, N. Roznyatovskaya, T. Herr, P. Fischer, The Chemistry of Redox-Flow Batteries, Angew. Chemie Int. Ed. 54 (2015) 9776–9809. doi:10.1002/anie.201410823.

[2] H. Chen, G. Cong, Y.C. Lu, Recent progress in organic redox flow batteries: Active materials, electrolytes and membranes, J. Energy Chem. 27 (2018) 1304–1325. doi:10.1016/j.jechem.2018.02.009.

[3] DOE Global Energy Storage Database, (n.d.). https://www.energystorageexchange.org/projects/1451 (accessed October 30, 2019).

[4] B. Dawoud, E. Amer, D. Gross, Vanadium redox flow batteries: a technological review, Int. J. Energy Res. 31 (2007) 135–147. doi:10.1002/er.

[5] V. Viswanathan, A. Crawford, D. Stephenson, S. Kim, W. Wang, B. Li, G. Coffey, E. Thomsen, G. Graff, P. Balducci, M. Kintner-Meyer, V. Sprenkle, Cost and performance model for redox flow batteries, J. Power Sources. 247 (2014) 1040–1051. doi:10.1016/j.jpowsour.2012.12.023.

[6] K. Gong, Q. Fang, S. Gu, S.F.Y. Li, Y. Yan, Nonaqueous redox-flow batteries: organic solvents, supporting electrolytes, and redox pairs, Energy Environ. Sci. 8 (2015) 3515–3530. doi:10.1039/C5EE02341F.

[7] Y. Huang, S. Gu, Y. Yan, S.F.Y. Li, Nonaqueous redox-flow batteries: features, challenges, and prospects, Curr. Opin. Chem. Eng. 8 (2015) 105–113. doi:10.1016/j.coche.2015.04.001.

[8] Y. Ding, C. Zhang, L. Zhang, Y. Zhou, G. Yu, Molecular engineering of organic

electroactive materials for redox flow batteries, Chem. Soc. Rev. 47 (2018) 69–103. doi:10.1039/c7cs00569e.

[9] T. Chu, I.A. Popov, G.A. Andrade, S. Maurya, P. Yang, E.R. Batista, B.L. Scott, R. Mukundan, B.L. Davis, Linked Picolinamide Nickel Complexes as Redox Carriers for Nonaqueous Flow Batteries, ChemSusChem. 12 (2019) 1304–1309. doi:10.1002/cssc.201802985.

[10] R.W. Hogue, K.E. Toghill, Metal Coordination Complexes in Non-Aqueous Redox Flow Batteries, Curr. Opin. Electrochem. 18 (2019) 37–45. doi:10.1016/j.coelec.2019.08.006.

[11] C.G. Armstrong, K.E. Toghill, Stability of molecular radicals in organic non-aqueous redox flow batteries: A mini review, Electrochem. Commun. 91 (2018) 19–24. doi:10.1016/j.elecom.2018.04.017.

[12] C.G. Armstrong, K.E. Toghill, Cobalt(II) complexes with azole-pyridine type ligands for non-aqueous redox-flow batteries: Tunable electrochemistry via structural modification, J. Power Sources. 349 (2017) 121–129. doi:10.1016/j.jpowsour.2017.03.034.

[13] R. Hogue, C. Armstrong, K. Toghill, Dithiolene Complexes of First Row Transition Metals for Symmetric Non-Aqueous Redox Flow Batteries, ChemSusChem. 12 (2019) 4506–4515. doi:10.1002/cssc.201901702.

[14] A.E.S. Sleightholme, A.A. Shinkle, Q. Liu, Y. Li, C.W. Monroe, L.T. Thompson, Non-aqueous manganese acetylacetonate electrolyte for redox flow batteries, J. Power Sources. 196 (2011) 5742–5745. doi:10.1016/j.jpowsour.2011.02.020.

[15] Q. Liu, A.A. Shinkle, Y. Li, C.W. Monroe, L.T. Thompson, A.E.S. Sleightholme, Non-aqueous chromium acetylacetonate electrolyte for redox flow batteries, Electrochem. Commun. 12 (2010) 1634–1637. doi:10.1016/j.elecom.2010.09.013.

[16] Q. Liu, A.E.S. Sleightholme, A.A. Shinkle, Y. Li, L.T. Thompson, Non-aqueous vanadium acetylacetonate electrolyte for redox flow batteries, Electrochem. Commun. 11 (2009) 2312–2315. doi:10.1016/j.elecom.2009.10.006.

[17] Y. Matsuda, K. Tanaka, M. Okada, Y. Takasu, M. Morita, T. Matsumura-Inoue, A rechargeable redox battery utilizing ruthenium complexes with non-aqueous organic electrolyte, J. Appl. Electrochem. 18 (1988) 909–914. doi:10.1007/BF01016050.

[18] H. seung Kim, S. Hwang, J. Mun, H. Park, J.H. Ryu, S.M. Oh, Counter anion effects on the energy density of Ni(II)-chelated tetradentate azamacrocyclic complex cation as single redox couple for non-aqueous flow batteries, Electrochim. Acta. 308 (2019) 227–230. doi:10.1016/j.electacta.2019.04.027.

[19] S. Hwang, H. seung Kim, J.H. Ryu, S.M. Oh, Ni(II)-chelated thio-crown complex as a single redox couple for non-aqueous flow batteries, Electrochem. Commun. 85 (2017) 36–39. doi:10.1016/j.elecom.2017.10.015.

[20] L.E. Vangelder, A.M. Kosswattaarachchi, P.L. Forrestel, T.R. Cook, E.M. Matson, Polyoxovanadate-Alkoxide clusters as multi-electron charge carriers for symmetric non-Aqueous redox flow batteries, Chem. Sci. 9 (2018) 1692–1699. doi:10.1039/c7sc05295b.

[21] C.G. Armstrong, R.W. Hogue, K.E. Toghill, Application of the dianion croconate violet for symmetric organic non-aqueous redox flow battery electrolytes, J. Power Sources.

440 (2019) 227037. doi:10.1016/j.jpowsour.2019.227037.

[22] T. Hagemann, J. Winsberg, B. Häupler, T. Janoschka, J.J. Gruber, A. Wild, U.S. Schubert, A bipolar nitronyl nitroxide small molecule for an all-organic symmetric redox-flow battery, NPG Asia Mater. 9 (2017). doi:10.1038/am.2016.195.

[23] W. Duan, R.S. Vemuri, J.D. Milshtein, S. Laramie, R.D. Dmello, J. Huang, L. Zhang, D. Hu, M. Vijayakumar, W. Wang, J. Liu, R.M. Darling, L. Thompson, K. Smith, J.S. Moore, F.R. Brushett, X. Wei, A symmetric organic-based nonaqueous redox flow battery and its state of charge diagnostics by FTIR, J. Mater. Chem. A. 4 (2016) 5448–5456. doi:10.1039/C6TA01177B.

[24] R.A. Potash, J.R. McKone, S. Conte, H.D. Abruña, On the benefits of a symmetric redox flow battery, J. Electrochem. Soc. 163 (2016) A338–A344. doi:10.1149/2.0971602jes.

[25] T. Ma, Z. Pan, L. Miao, C. Chen, M. Han, Z. Shang, J. Chen, Porphyrin-Based Symmetric Redox-Flow Batteries towards Cold-Climate Energy Storage, Angew. Chemie - Int. Ed. 57 (2018) 3158–3162. doi:10.1002/anie.201713423.

[26] D. Zhang, Q. Liu, X. Shi, Y. Li, Tetrabutylammonium hexafluorophosphate and 1-ethyl-3-methyl imidazolium hexafluorophosphate ionic liquids as supporting electrolytes for non-aqueous vanadium redox flow batteries, J. Power Sources. 203 (2012) 201–205. doi:10.1016/j.jpowsour.2011.10.136.

[27] A.A. Shinkle, A.E.S.S. Sleightholme, L.D. Griffith, L.T. Thompson, C.W. Monroe, Degradation mechanisms in the non-aqueous vanadium acetylacetonate redox flow battery, J. Power Sources. 206 (2012) 490–496. doi:10.1016/j.jpowsour.2010.12.096.

[28] T. Herr, J. Noack, P. Fischer, J. Tübke, 1,3-Dioxolane, tetrahydrofuran, acetylacetone

and dimethyl sulfoxide as solvents for non-aqueous vanadium acetylacetonate redox-flow-batteries, Electrochim. Acta. 113 (2013) 127–133. doi:10.1016/j.electacta.2013.09.055.

[29] A. a. Shinkle, T.J. Pomaville, A.E.S. Sleightholme, L.T. Thompson, C.W. Monroe, Solvents and supporting electrolytes for vanadium acetylacetonate flow batteries, J. Power Sources. 248 (2014) 1299–1305. doi:10.1016/j.jpowsour.2013.10.034.

[30] T. Herr, P. Fischer, J. Tübke, K. Pinkwart, P. Elsner, Increasing the energy density of the non-aqueous vanadium redox flow battery with the acetonitrile-1,3-dioxolane-dimethyl sulfoxide solvent mixture, J. Power Sources. 265 (2014) 317–324. doi:10.1016/j.jpowsour.2014.04.141.

[31] I.L. Escalante-Garcia, J.S. Wainright, L.T. Thompson, R.F. Savinell, Performance of a Non-Aqueous Vanadium Acetylacetonate Prototype Redox Flow Battery: Examination of Separators and Capacity Decay, J. Electrochem. Soc. 162 (2014) A363–A372. doi:10.1149/2.0471503jes.

[32] M.O. Bamgbopa, N. Pour, Y. Shao-Horn, S. Almheiri, Systematic selection of solvent mixtures for non-aqueous redox flow batteries – vanadium acetylacetonate as a model system, Electrochim. Acta. 223 (2017) 115–123. doi:10.1016/j.electacta.2016.12.014.

[33] J.D. Milshtein, J.L. Barton, R.M. Darling, F.R. Brushett, 4-Acetamido-2,2,6,6-tetramethylpiperidine-1-oxyl as a model organic redox active compound for nonaqueous flow batteries, J. Power Sources. 327 (2016) 151–159. doi:10.1016/j.jpowsour.2016.06.125.

[34] J.D. Milshtein, J.L. Barton, T.J. Carney, J.A. Kowalski, R.M. Darling, F.R. Brushett, Towards low resistance nonaqueous redox flow batteries, J. Electrochem. Soc. 164 (2017) A2487–A2499. doi:10.1149/2.0741712jes.

[35] L. Cosimbescu, X. Wei, M. Vijayakumar, W. Xu, M.L. Helm, S.D. Burton, C.M. Sorensen, J. Liu, V. Sprenkle, W. Wang, Anion-Tunable Properties and Electrochemical Performance of Functionalized Ferrocene Compounds, Sci. Rep. 5 (2015) 14117. doi:10.1038/srep14117.

[36] X. Wei, L. Cosimbescu, W. Xu, J.Z. Hu, M. Vijayakumar, J. Feng, M.Y. Hu, X. Deng, J. Xiao, J. Liu, V. Sprenkle, W. Wang, Towards High-Performance Nonaqueous Redox Flow Electrolyte Via Ionic Modification of Active Species, Adv. Energy Mater. 5 (2015) n/a-n/a. doi:10.1002/aenm.201400678.

[37] S. Hwang, H. seung Kim, J.H. Ryu, S.M. Oh, N-ferrocenylphthalimide; A single redox couple formed by attaching a ferrocene moiety to phthalimide for non-aqueous flow batteries, J. Power Sources. 395 (2018) 60–65. doi:10.1016/j.jpowsour.2018.05.053.

[38] K. Park, J.H. Cho, K. Shanmuganathan, J. Song, J. Peng, M. Gobet, S. Greenbaum, C.J. Ellison, J.B. Goodenough, New battery strategies with a polymer/Al2O3 separator, J. Power Sources. 263 (2014) 52–58. doi:10.1016/j.jpowsour.2014.04.017.

[39] Q. Huang, H. Li, M. Grätzel, Q. Wang, Reversible chemical delithiation/lithiation of LiFePO4: Towards a redox flow lithium-ion battery, Phys. Chem. Chem. Phys. 15 (2013) 1793–1797. doi:10.1039/c2cp44466f.

[40] J.D. Milshtein, A.P. Kaur, M.D. Casselman, J.A. Kowalski, S. Modekrutti, P.L. Zhang, N.H. Attanayake, C.F. Elliott, S.R. Parkin, C. Risko, F.R. Brushett, S.A. Odom, High

current density, long duration cycling of soluble organic active species for non-aqueous redox flow batteries, Energy Environ. Sci. 9 (2016) 3531–3543. doi:10.1039/C6EE02027E.

[41] K.H. Hendriks, C.S. Sevov, M.E. Cook, M.S. Sanford, Multielectron cycling of a low-potential anolyte in alkali metal electrolytes for nonaqueous redox flow batteries, ACS Energy Lett. 2 (2017) 2430–2435. doi:10.1021/acsenergylett.7b00559.

[42] N.H. Attanayake, J.A. Kowalski, K. V. Greco, M.D. Casselman, J.D. Milshtein, S.J. Chapman, S.R. Parkin, F.R. Brushett, S.A. Odom, Tailoring Two-Electron-Donating Phenothiazines to Enable High-Concentration Redox Electrolytes for Use in Nonaqueous Redox Flow Batteries, Chem. Mater. 31 (2019) 4353–4363. doi:10.1021/acs.chemmater.8b04770.

[43] A. Forner-Cuenca, E.E. Penn, A.M. Oliveira, F.R. Brushett, Exploring the Role of Electrode Microstructure on the Performance of Non-Aqueous Redox Flow Batteries, J. Electrochem. Soc. 166 (2019) A2230–A2241. doi:10.1149/2.0611910jes.

[44] N.G. Connelly, W.E. Geiger, Chemical redox agents for organometallic chemistry, Chem. Rev. 96 (1996) 877–910. doi:10.1021/cr940053x.

[45] J.D. Milshtein, K.M. Tenny, J.L. Barton, J. Drake, R.M. Darling, F.R. Brushett, Quantifying Mass Transfer Rates in Redox Flow Batteries, J. Electrochem. Soc. 164 (2017) E3265–E3275. doi:10.1149/2.0201711jes.

[46] D. Astruc, Why is Ferrocene so Exceptional?, Eur. J. Inorg. Chem. 2017 (2017) 6–29. doi:10.1002/ejic.201600983.

[47] R.R. Gagne, C.A. Koval, G.C. Lisensky, Ferrocene as an Internal Standard for

Electrochemical Measurements, Inorg. Chem. 19 (1980) 2854–2855. doi:10.1021/ic50211a080.

[48] B. Hwang, M.-S.S. Park, K. Kim, Ferrocene and cobaltocene derivatives for non-aqueous redox flow batteries, ChemSusChem. 8 (2015) 310–314. doi:10.1002/cssc.201403021.

[49] M. Malischewski, M. Adelhardt, J. Sutter, K. Meyer, K. Seppelt, Isolation and structural and electronic characterization of salts of the decamethylferrocene dication, Science (80-.). 353 (2016) 678–682. doi:10.1126/science.aaf6362.

[50] J. Yuan, C. Zhang, Y. Zhen, Y. Zhao, Y. Li, Enhancing the performance of an all-organic non-aqueous redox flow battery, J. Power Sources. 443 (2019) 227283. doi:10.1016/j.jpowsour.2019.227283.

[51] F. Yang, D. Wang, Y. Zhao, K.L. Tsui, S.J. Bae, A study of the relationship between coulombic efficiency and capacity degradation of commercial lithium-ion batteries, Energy. 145 (2018) 486–495. doi:10.1016/j.energy.2017.12.144.

[52] A. Singh, D.R. Chowdhury, A. Paul, A kinetic study of ferrocenium cation decomposition utilizing an integrated electrochemical methodology composed of cyclic voltammetry and amperometry, Analyst. 139 (2014) 5747–5754. doi:10.1039/c4an01325e.

[53] J.P. Hurvois, C. Moinet, Reactivity of ferrocenium cations with molecular oxygen in polar organic solvents: Decomposition, redox reactions and stabilization, J. Organomet. Chem. 690 (2005) 1829–1839. doi:10.1016/j.jorganchem.2005.02.009.

[54] G. Zotti, G. Schiavon, S. Zecchin, D. Favretto, Dioxygen-decomposition of ferrocenium

molecules in acetonitrile: The nature of the electrode-fouling films during ferrocene electrochemistry, J. Electroanal. Chem. 456 (1998) 217–221. doi:10.1016/S0022-0728(98)00279-4.

[55] A. Singh, D.R. Chowdhury, A. Paul, A kinetic study of ferrocenium cation decomposition utilizing an integrated electrochemical methodology composed of cyclic voltammetry and amperometry, Analyst. 139 (2014) 5747–5754. doi:10.1039/c4an01325e.

[56] J.D. Saraidaridis, C.W. Monroe, Nonaqueous vanadium disproportionation flow batteries with porous separators cycle stably and tolerate high current density, J. Power Sources. 412 (2019) 384–390. doi:10.1016/j.jpowsour.2018.11.058.

[57] B. Ok, W. Na, T.H. Kwon, Y.W. Kwon, S. Cho, S.M. Hong, A.S. Lee, J.H. Lee, C.M. Koo, Understanding the enhanced electrochemical performance of TEMPO derivatives in non-aqueous lithium ion redox flow batteries, J. Ind. Eng. Chem. 80 (2019) 545–550. doi:10.1016/j.jiec.2019.08.027.

[58] M. Taggougui, B. Carré, P. Willmann, D. Lemordant, Application of a nitroxide radical as overcharge protection in rechargeable lithium batteries, J. Power Sources. 174 (2007) 643–647. doi:10.1016/j.jpowsour.2007.06.124.

[59] J.F. Kucharyson, L. Cheng, S.O. Tung, L.A. Curtiss, L.T. Thompson, Predicting the potentials, solubilities and stabilities of metal-acetylacetonates for non-aqueous redox flow batteries using density functional theory calculations, J. Mater. Chem. A. 5 (2017) 13700–13709. doi:10.1039/C7TA01285C.